The use of synchrotron x-rays to observe copper corrosion in real time.

Mark Dowsett[1], Annemie Adriaens[2,*] Chris Martin[3] and L. Bouchenoire[4,5]

[1] Department of Physics, University of Warwick, Coventry CV4 7AL, UK

[2] Department of Analytical Chemistry, Ghent University, Krijgslaan 281-S12, Ghent, Belgium

[3] School of Materials, University of Manchester, Oxford Road, Manchester M13 9PL, UK

[4] European Synchrotron Radiation Facility, XMaS Beamline, 6 Rue Jules Horowitz, BP220, 38043 Grenoble, Cedex, France

[5] Department of Physics, University of Liverpool, Liverpool L69 7ZE, UK

[*] Corresponding author: annemie.adriaens@ugent.be, Fax +32 9 264 4960

Abstract

We have developed and tested two complementary methods for making time-lapse synchrotron X-ray diffraction (XRD) measurements of the growth of synthetic corrosion layers using a protocol for producing copper (I) chloride (nantokite), on copper as a test. In the first method a copper coupon was spin-coated with saturated copper (II) chloride solution in air whilst the surface was characterized in real time using XRD with a fast 1-D detector. In the second, a droplet of the same reagent was suspended from an X-ray transparent window in a hermetically sealed cell and the coupon was brought into contact with this whilst XRD diffractograms were acquired with a CCD camera. The protocol is completed by a deionized water rinse which was also studied. The XRD shows nantokite precipitation in solution as well as growth on the surface, but the end products were variable proportions of nantokite cuprite, and paratacamite. The latter two were observed forming in a reaction between the nantokite and the rinsing water. Comparisons between samples analyzed in the synchrotron and at lower power densities show that the effects of any radiolysis or slight heating of the sample are insignificant in this case. It would be simple to extend these methods to other corrosion or surface reaction systems.

Keywords: Synchrotron, time-lapse spectroscopy, copper, corrosion, conservation

Introduction

Synchrotrons provide intense, monochromatic, beams of x-rays containing 10^4 or more times the flux from a laboratory source, and allow the user to select an energy in the 1 - 100 keV range. The combination of the high flux (and flux density) with fast detection systems makes them ideal for the *in-situ* study of evolving chemical systems using techniques such as x-ray fluorescence[1], x-ray absorption spectrocopy (XAS) [2-5], transmission x-ray microscopy[6], and x-ray diffraction (XRD)[7-9] or some combination[10]. X-rays can penetrate a thickness of liquid which increases with energy, and which is a millimetre or more from energies of a few keV upwards. It is therefore possible to observe the chemical reactions on surfaces immersed in liquids with a time resolution down to a few milliseconds[7] limited by detector speed, counting statistics, and other factors depending on the particular spectroscopy involved (e.g. the speed with which the monochromator can be scanned over the energy range required in XAS). Potentially, information on the evolving chemistry and structure of both the liquid and the surface are available[3]. The development of cells in which a chemical process may be invoked, electrochemically or otherwise, has therefore been a feature of synchrotron science since 1980[11]. Some degree of automation is required since human presence in the experimental hutch when the x-rays are on is exceptionally hazardous and strictly forbidden. So, for example, where the chemical change to be studied commences on contact between the surface and the reagent, this is ideally initiated under remote control and synchronized with the start of data acquisition so that no stage of the process is lost. How this may be done depends on the nature of the experiment. The work reported here was carried out as part of the development of experimental procedures for corrosion protocol testing and subsequent evaluation of surface protection or passivation techniques. These are intended to include means to both observe the reactions as they happen, identify the end products and understand their origins. Research in recent years[e.g. 3, 12] has shown that, although many corrosion protocols exist in the literature, it is wise to test them in the context in which they are to be used and check that they produce the corrosion products expected in a useful form. A complex set of by-products can result if essential parameters such as ambient temperature and relative humidity go unreported or where initial treatment with a corrosive agent is followed by an ill-defined period of air or water exposure (e.g. rinsing).

In this paper we focus on the corrosion of copper to form nantokite (copper (I) chloride). We work with realistic heterogeneous surfaces where the starting condition is typical of routinely polished polycrystalline metal (r.m.s. roughness > 1μm), this becomes pitted during corrosion, and the corrosion products are rough to the eye. Nantokite is a naturally occurring corrosion product found on cupreous artifacts, especially those exposed to marine environments[13]. The pitting and continued damage it causes are well known in both ancient and modern contexts[13,14]. Nantokite can be artificially made using protocols which are relatively simple and predictable compared to those used for other cupreous compounds (e.g. the hydroxychlorides[3]) and therefore we use it here to establish two complementary time-lapse methods which involve (i) spin coating a metal coupon with a corrosive reagent in the beam line and acquiring XRD data from the evolving surface and (ii) distributing a droplet of corrosive reagent on a coupon surface under anaerobic conditions and acquiring real time XRD from the moment of contact. In case (i) the corroding surface is also exposed to the air and therefore subject to evaporation andexposed to other oxidants. This is a very common corrosion scenario. In case (ii), evaporation is prevented and exposure to air is limited to diffusion through the window. As a side benefit, the work has enabled us to understand a previously published experiment[15] more completely.

Experimental

Synthetic corrosion protocol

Nantokite corrosion layers were grown on 2 mm thick, 12.5 mm diameter coupons made from 99.9 % pure copper (Goodfellow Cambridge, UK and Advent Research Materials, UK). Prior to use, the coupons were mechanically cleaned with P1200 grit silicon carbide (SiC) abrasive paper wetted to prevent clogging, to expose a fresh metal surface. This was rinsed with deionized water then ultrasonically cleaned in 2-propanol for 15 minutes. At no stage was water allowed to dry out on the surface, as this tends to leave drying stains containing abrasive and also cuprite. Surfaces were subsequently polished by hand using a hydroentangled polyethylene wipe (DuPont) loaded with a 1 μm alumina water suspension. To remove adherent alumina particles, coupons were rinsed then ultrasonically cleaned in 2-propanol for 15 minutes (no water was used

in this stage of the cleaning). Use of the coupon commenced a few minutes after this process was complete.

The protocol for preparing and applying the corrosive solution was adapted from aesthetically oriented literature[16] which gives recipes for producing decorative patinas on metals and an internal report from a restoration laboratory[17] aimed at adapting these for controlled studies. Nantokite was prepared using a saturated solution of copper (II) chloride made by adding > 78 g of $CuCl_2.2H_2O$ (Aldrich) per 100 mL of deionized water. Normally, copper coupons are dipped in this for around an hour whilst ensuring that the solution remains saturated. Then the coupon is removed and rinsed in deionized water. For the time-lapse experiments described below, drops of the solution were automatically dispensed onto the surface of a coupon. This approach produced no difference in the final reaction products. The result is a thin layer of corrosion product which varies in color between black, grey, yellow and light green.

High-resolution time-lapse XRD

SR-XRD experiments were carried out using station MPW6.2 at the Synchrotron Radiation Source (SRS, Daresbury, UK)[18] and BM28 (XMaS)[19] at the European Synchrotron Radiation Facility. Although the SRS is now closed, similar facilities are available at many synchrotrons. On both beam lines, the beam was incident at 10° to the sample surface with an elliptical footprint around 0.5 mm wide and 3 mm long (beam width and height 0.5 mm).

On MPW 6.2, a monochromatic beam ~10^{12} photons mm^{-2} s^{-1} with a wavelength of 1.4 Å was used. Data were acquired using the RAPID II detector system[20]. The diffracted beam is collected over 60º simultaneously (a range of ~6º to ~66º for these experiments), along an arc 384 mm long with 4096 individual elements. A fast shutter was placed in the beam so that the samples were only irradiated whilst patterns were being recorded. The opening and closing time were insignificant on the timescale of the exposures used here. The growth of the corrosion product was done *in-situ* in the beam line by using a custom designed open chemical reactor (eSpin). This can automatically dispense a corrosive medium onto a rapidly rotating surface during X-ray analysis (Figure 1). It consists of a PCTFE cup with inner and outer diameters of

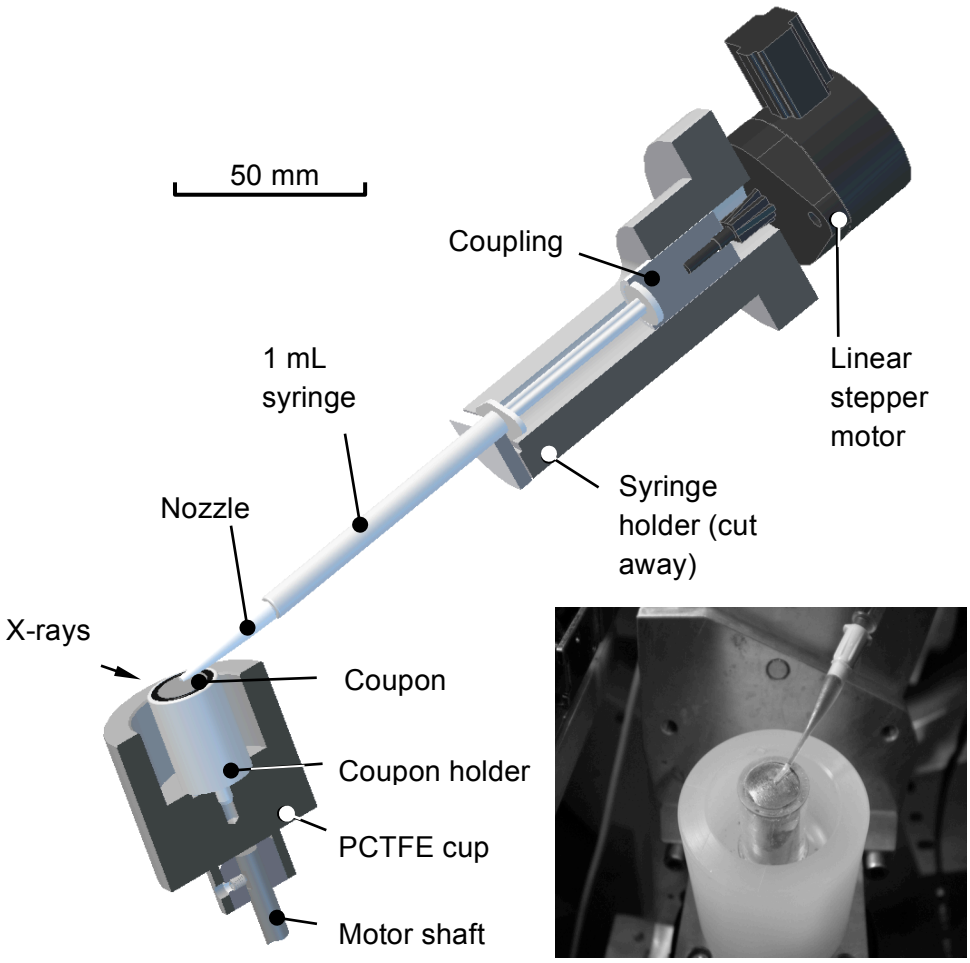

Figure 1. Schematic of eSpin device with photograph of nantokite production (inset).

30 and 44 mm respectively, configured to take electrodes or coupons with a diameter of 12.6 mm in a holder from which they can easily be demounted. The device is driven by a variable speed motor (type BLDC 58, McLennan Servo Supplies Ltd., UK), whose speed can be varied between 0 and 3650 rpm by remote control from outside the X-ray hutch. It comes together with a 1 mL syringe mounted on a flexible arm, which allows the tip of the syringe to be positioned close to the sample. In the experiments described here, the syringe was fitted with a 1 mm bore polyethylene nozzle cut parallel with the sample surface so that it acted as a wiper (similar results were obtained with a straight nozzle and a wiper made from polyimide tape (Kapton®, DuPont)). This was found to be necessary in order to distribute the liquid evenly over the polished copper surface and to keep the film thickness sufficiently low for X-rays to penetrate. The copper peaks are typically attenuated by a factor of 8 the moment the solution is dispensed. Using online tools[21] and for a solution of initial composition 0.75 g cm^{-3} $CuCl_2$ (i.e. a saturated solution, and ignoring the attenuation of the water) it can be shown that the total X-ray path length is ~400-500 μm. Allowing for an entry path at 10° and an exit path at 45°, this gives a liquid film thickness around 65 μm. At the same time the drops of solution dispensed "pile up" around the wiper and this volume acts as a dispenser to the rotating sample surface over time. The syringe is driven by a linear stepper motor (type UBL23, Saia-Burgess Ltd., UK), which is also controlled remotely from outside the X-ray hutch. Therefore XRD acquisition can be started on a clean sample surface and single or sequenced drops of liquid can then be dispensed onto the sample while taking data. The sample surface and the dispersion of the fluid onto the sample were recorded in real time using a web-cam.

In preliminary experiments, speeds of 150-300 r.p.m. were found to be the most satisfactory for liquid distribution in this case. With the sample mounted in eSpin but protected by a sheet of thermoplastic film (Parafilm M®, Alpha Laboratories Ltd., UK), the syringe was loaded with the protocol solution and put into position so that the cut nozzle extended radially across the sample (Figure 1, inset). The film was removed just before the experimental hutch was closed up prior to the opening of the main X-ray shutter. The Rapid II detector was programmed to take 500 XRD measurements accumulating for 2 s each with a 2 s interval between. Three drops of solution (approx. 0.15 mL) were dispensed in the first 12 measurements, and the reaction was then left to take its course for a total of 2000s. Sample rotation was maintained throughout the acquisition.

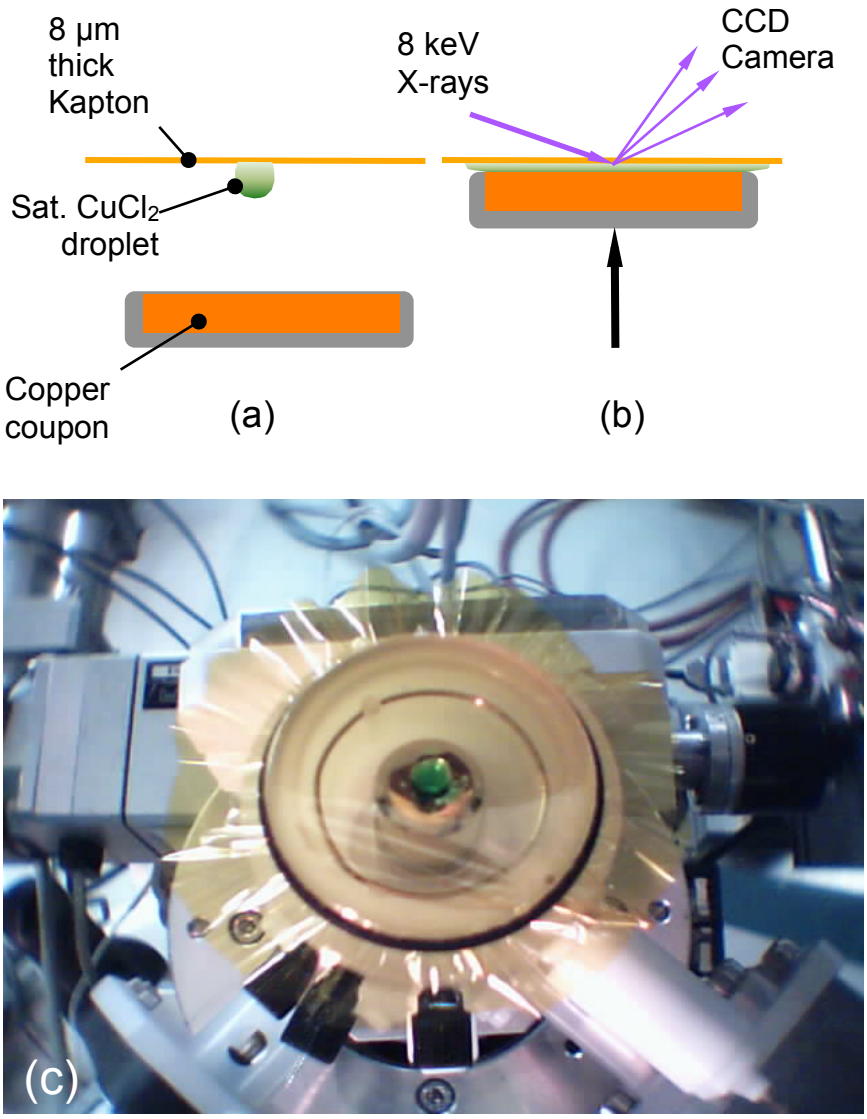

Figure 2. (a) Droplet of saturated copper (II) chloride suspended from cell window.
(b) Coupon moved into contact with droplet by stepper motor.
(c) Moment of contact captured by webcam.

On XMaS, the measurements were made using a Mar CCD 165 camera (Mar USA Inc.) which provides 2-D diffractograms containing supplementary information on granularity and preferred orientation in comparison to the 1-D detector above (although angular resolution is sacrificed because of the open geometry required). The 8 keV (1.5498 Å) beam was of comparable power density and total flux to that from MPW 6.2. The camera axis was at 45º to the input beam so that the intersection between the Scherrer cones and the camera surface was elliptical. The camera surface was 130 mm from the sample centre (*d* in Supporting Information, Figure S-1). Time-lapse experiments were performed using similar total X-ray dose at the same power density as in the Rapid II measurements, but without spinning the sample. Instead the following method was used: a drop (0.05 mL) of reagent was suspended from the inside of an 8 μm thick X-ray transparent polyimide window (PANalytical BV) on an electrochemical/environmental cell (eCell) described elsewhere[9,22] (Figure 2). A copper coupon mounted on the remote controlled sample holder in the cell was raised into contact with the drop which was spread over the surface as the coupon was brought to within 150 μm of the window (Figure 2(a)(b)). The reagent was sandwiched between the coupon and the window so that there was no significant contact with the atmosphere compared to the experiments above. XRD measurements commenced as the drop was deformed by contact (Figure 2(c)) using a 5 second exposure and a 6 second interval between images. After the diffractograms had stopped changing, the window was removed and the coupon was allowed to dry in air whilst data taking continued. End points in both the above experiments were compared to sample surfaces which had been prepared without X-irradiation, and rinsed in the normal way.

Data processing

The Mar images and Rapid II patterns were processed using esaProject[23] (© 2006 Mark Dowsett), which provides an acquisition to publishing capability for XRD, X-ray absorption spectroscopy (XAS), X-ray excited optical luminescence (XEOL), and other spectroscopic data with image stack and spectrum/diffraction pattern data manipulation and mining features. (See Supporting Information Figures S-1 and S-2) XRD patterns were interpreted using references from the MinCryst[24,25] and International Centre For Diffraction Data (ICDD)[266] databases.

Results and discussion

For ease of comparison between Rapid II, and Mar data, the abscissae of all XRD patterns are transformed to a wave number scale Q where

$$Q = \frac{2\pi}{d} = \frac{4\pi \sin\Theta}{\lambda}, \quad (1)$$

d is the interatomic plane spacing, 2Θ is the scattering angle, and λ is the X-ray wavelength. Some patterns have been plotted using a conventional square root intensity scale to enhance the visibility of small peaks.

Influence of the beam

The photon intensity at station MPW6.2 was ~1.7 x 10^{11} mm^{-2} s^{-1} when projected onto the sample at 10º. This is around 1000 times higher than in our previous investigations on this system[15,22] and over 10000 times higher than for a laboratory diffractometer. Although the measurement time per pattern is correspondingly shortened from several hours to ≤ 5 s due both to the total flux and the parallel collection, we were concerned that the power density might modify the results of the protocols in the time-lapse experiments. The stability of the end products was tested in a set of experiments in which sets of 30 SR-XRD patterns each were acquired on various areas of a pre-corroded copper sample. Each pattern involved irradiation for between 1 and 10 seconds, making a total exposure of up to 300 s per set. The SR-XRD showed no evolution with dose, indicating that the incident beam was not changing the surface composition of the sample under study. It is generally more difficult to determine whether radiolysis of the solution by the X-radiation is modifying the effect of a protocol. In the case of nantokite reported here, the end-products were the same for the time-lapse SR-XRD and laboratory XRD measurements made after the application of the protocol, apart from variations due to orientational effects which occurred irrespective of the analytical method.

Evolution of the corrosion layer

The protocol for nantokite is relatively simple, and the nantokite is formed through

$$Cu + CuCl_2 \rightarrow 2CuCl \quad (2)$$

We found no evidence to suggest that the radiolysis of the copper chloride solution, the perturbation due to spinning against a wiper blade, or the air exposure affected the outcome. Figure 3 shows a waterfall plot of the time-lapse data from an eSpin experiment obtained on MPW6.2 in the first 2000 seconds of reaction. Every 5th pattern is shown. Note that, at the end of this time, the surface of the sample was still wet. A slight change in background level and a large drop in the copper signal (which allows the solution thickness under the beam to be established as ~65 μm - see Experimental section) marks the point at which the drops of copper (II) chloride solution were added. The Cu (220) reflection is attenuated less than the other Cu peaks because it has a shorter escape path. Only nantokite is produced in this stage of the protocol, and nantokite reflections become detectable in the system immediately and increase in strength whilst the copper reflections almost disappear. If all the $CuCl_2$ in an initial 65 μm layer of solution were to be converted to a CuCl precipitate on the surface and in suspension (mean density of CuCl 1.11 g cm^{-3} in the same thickness), one would expect a progressive decrease of intensity in the Cu reflections of a factor of ~1.8 from reference 21. In Figure 3 the Cu(220) peak decreases by a factor of 6 from the point immediately after the addition of the solution to a point 1000s into the exposure, after which the intensity increases a small amount. This is due probably due to redistribution of solution piled behind the wiper on the spinning sample over time, and the resulting deposition of further CuCl under the beam. Furthermore, if the liquid medium is allowed to dry (in a departure from the normal protocol) as discussed below, the copper peaks re-emerge, and they are visible in any case after the protocol is complete[15,22]. From these observations we deduce that the slow copper attenuation following initial dispensation is due both to absorption in the surface liquid which becomes rich in copper ions and then precipitated nantokite, and to the formation of the nantokite deposit. The precipitate is visible to the eye when copper is immersed in a larger volume of saturated copper (II) chloride solution, when it can be observed as a dark suspension emerging like smoke from the surface. A very

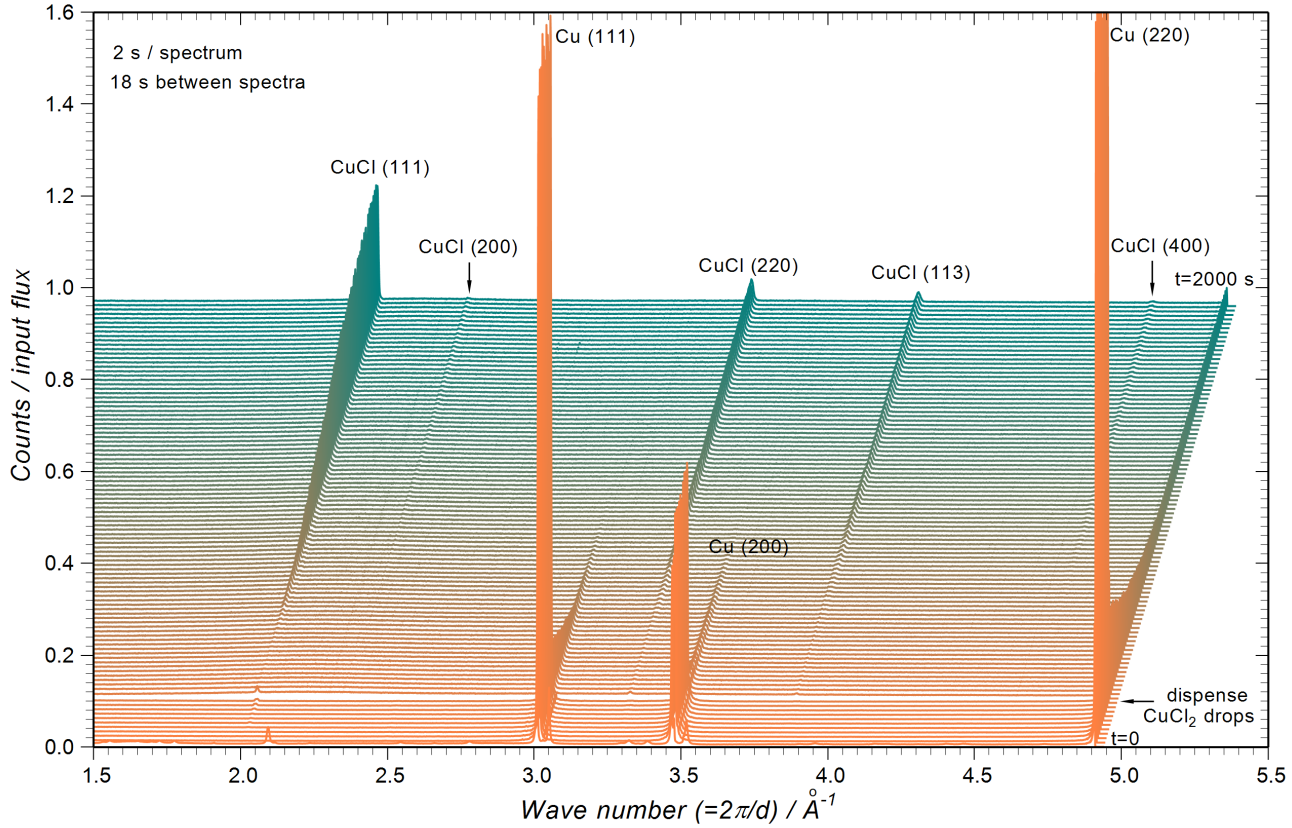

Figure 3: Waterfall plot of the Rapid II time-lapse SR-XRD patterns acquired during the nantokite protocol. (100 patterns from set of 500.) Each pattern took 2 s to acquire.

similar result is observed in the droplet experiment on XMaS, with the exception that the copper reflections remain visible because the liquid layer is much thinner (see also Figure S-3).

In a departure from the normal protocol, and to explore aspects of the experimental method, we observed the effect of allowing the liquid to dry out on the surface following a droplet experiment on XMaS. This was done by simply removing the window on the cell and recommencing the data acquisition using the Mar camera. (Typical Mar images from this experiment in comparison with the growth and rinsing stages are shown in S-4) In Figure 4(a) we show a time lapse image of 50 patterns which were extracted from a corresponding sequence of Mar diffractograms taken over ~600 seconds whilst the surface was drying. The intensity in each pattern has been used to modulate the grey scale in a corresponding row of the image displayed so that the bottom row corresponds to time=0 etc. (the corresponding waterfall plot is given in Supporting Information, Figure S-5). Figure 4(b) shows the pattern used to make the top row of the image in Figure 4(a). The crystallization of excess copper (II) chloride as eriochalcite is evident [$CuCl_2.2H_2O$] (peaks labeled E and (E). Reflections labeled (E) were present in the XRD from the $CuCl_2$ used to make the solution, but not in the database eriochalcite pattern. (Reference patterns[24] are given in Supporting Information, Figure S-6.) Copper, Cu, and nantokite, N, reflections are also clearly visible.

Figure 4(a) also shows significant changes in peak shape over time, with peak splitting occurring for the copper and nantokite reflections between 2.95 and 3.95 $Å^{-1}$ as the layer dries out. The splitting results from a displacement of a reflection of up to 840 μm on the camera face. Peak shifts due to changes in scattering angle of a few tenths of a degree would account for this, and such have been observed due to refraction of X-rays in a thin surface layer[27]. However, these were seen at grazing incidence of $\leq 1°$ on atomically flat surfaces and decreased below 0.1° with increasing angle of incidence. Our incident angle is 10°, the substrate surface is rough on the micron scale because of its preparation and pitting during corrosion, and the corrosion layer is visibly rough. Even if refraction effects are present, they are unlikely, therefore, to be observable here. We therefore interpret the observations as being due to increases in thickness of the corrosion crust and and stratification therein.

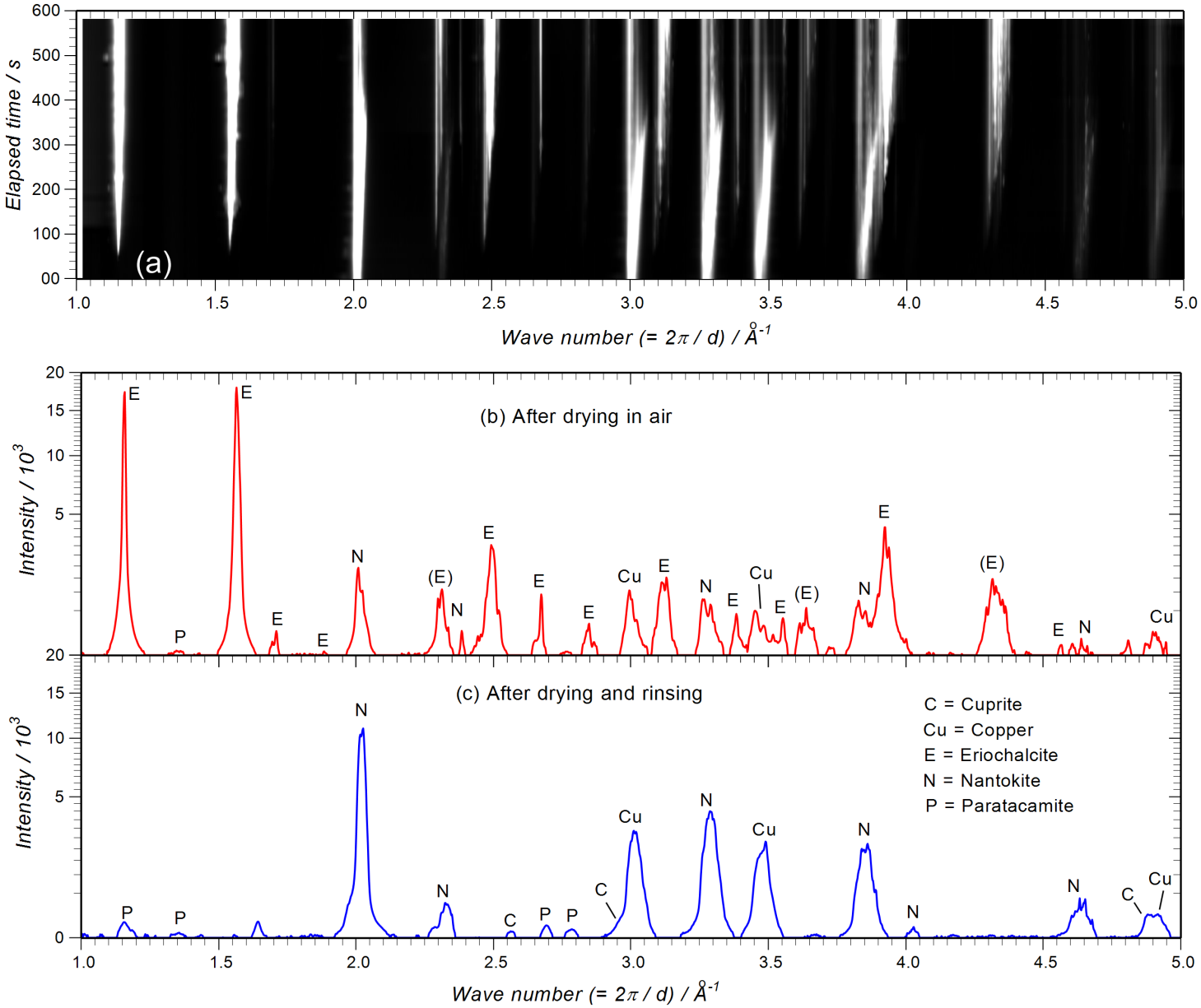

Figure 4: (a) Fifty patterns taken from a sequence of Mar diffractograms acquired as the residual copper (II) chloride solution from the protocol was allowed to dry in air. The acquisition time per diffractogram was 5 s. Each pattern has been used to modulate a linear grey scale to form one row of the image in (a). (b) The last pattern from the sequence in (a) (top row of the image). (c) A pattern taken after rinsing the sample. The intensity is plotted on a square root scale. Reference patterns[24], are shown in Supporting Information Figure S-6. Reflections labeled (E) were present in the XRD from the $CuCl_2$ used to make the solution, but not in the database eriochalcite pattern.

For the geometry we use here (Supporting Information Figure S-1) it can be shown that, for scattering in the plane defined by the beam and the camera axis, the displacement *h'* on the camera face due to diffraction from either end of the beam footprint is:

$$h' = h\frac{\sin(2\Theta - i)}{\sin i\ \cos(2\Theta - \beta)}, \tag{3}$$

where h is the height of the beam, i is the angle of incidence, and β is the angle between the beam and the camera axis. The beam is assumed to be essentially parallel. For i=10°, β=45° and a camera face 161.8 mm diameter positioned 130 mm from the sample the extremes are 6.2h at the top of the camera face and 0.37h at the bottom. A similar relationship holds for the displacement on the camera face *t'* due to reflection from the top and bottom of a thin layer of thickness t, or regions on the sample at different levels separated by t normal to the sample surface:

$$t' = t\frac{\sin 2\Theta}{\sin i\cos(2\Theta - \beta)} \tag{4}$$

In the case of the copper, the reflections at 3.0 $Å^{-1}$ and 3.47 $Å^{-1}$ broaden into a geometrically similar forked structure in the first 300 s, then gradually revert to a narrow line in the original position by the end of the measurement. In the first 150 seconds, the copper intensity rises by a factor of 1.7, and then decays to half its initial value by 600 seconds. (This is seen more clearly in Supporting Information, Figure S-5.) The separation of the components of the reflection at 3.0 $Å^{-1}$ on the camera face was 1.4 mm overall, and the value of 2Θ at the acquisition energy (8 keV) was 43.7°.

These effects are consistent with an initial redeposition of copper (a well known phenomenon in copper corrosion[13,28,29]) resulting in stratification in the surface layer with copper being observed from the substrate surface, but also in regions up to 350 μm above this (rearranging equation (4) to find t). These layers then recorrode and disappear leaving the intensity of the surface peak weakened by absorption. The non-uniformity in thickness of the corrosion product is evident from the fact that absorption by a uniform layer of either $CuCl$ or $CuCl_2.2H_2O$ >40 μm thick would render the substrate copper peak invisible[21], and this does not happen because the layer is patchy and rough. The nantokite reflections at 3.28 $Å^{-1}$ and 3.88 $Å^{-1}$ behave in a similar way, but bifurcation of the peaks is visible to the end showing persistent stratification in the nantokite. With regard to the eriochalcite peaks which are distributed across the diffraction pattern: Their

increasing width with increasing scattering angle is partly a consequence of equation (3) (finite footprint of the beam and intersection with a flat, rather than a cylindrical detector surface). This geometrical effect will also magnify actual changes in the peak width with time at high 2θ compared to low. The reflection at 3.93 $Å^{-1}$ in Figure 4(a) broadens with time and is significantly wider after 600 seconds than can be accounted for by equation (3) alone. The width on the camera face is 2.8 mm (original scattering angle 57.2°), and equation (3) accounts for 2.2 mm of this. Assuming that the remainder is due to height and thickness variations, equation (4) gives these at~130 μm. At the end of the drying, the surface corrosion consists of a rough patchy layer of eriochalcite with nantokite on the copper surface and also above the eriochalcite.

The purpose of the rinsing stage of the protocol is to remove excess copper (II) chloride whilst it is still in solution (and incidentally) much of the unattached nantokite. A similar result is obtained by rinsing the surface produced above as shown by Figure 4(c). The nantokite reflections become stronger possibly through further reaction of the surface during rinsing. Unfortunately, whether the surface is rinsed from dry, or immediately after removal from the solution, cuprite and paratacamite peaks also appear in varying proportion.

Nantokite, although it is insoluble, hydrolyses rapidly in water to form cuprite [Cu_2O] through

$$2CuCl + H_2O \rightarrow Cu_2O + 2HCl \qquad (5)$$

provided the pH of the system remains above 5.65 [30] (See also Figure S-7). In the presence of oxygen, paratacamite can also be formed[13]:

$$4CuCl + O_2 + 4H_2O \rightarrow 2Cu_2(OH)_3Cl + 2HCl \qquad (6)$$

Conclusions

Using the eSpin device and the two second pattern acquisition time possible with the RAPID II detector at SRS we were able to obtain sets of time-lapse XRD patterns covering a corrosion process from the first contact between a corrosive liquid and a metal surface, and the subsequent

evolution until the reaction ceased. An alternative experiment performed by trapping a droplet of reagent between a thin polymer window and the metal surface and using a Mar CCD camera to collect 2-D diffraction patterns with a five second acquisition time on the XMaS beam line at ESRF gave similar results. Further stages in a corrosion protocol (drying in air and rinsing) were monitored. Overall, the methods described here are applicable in many areas, but measurements using low power densities at key points in the reactions are advisable to identify any effects of radiolysis or heating in the synchrotron beam. For the nantokite protocol examined here, no effect attributable to the intense X-ray beams was seen. As Figure 3 shows, the data were considerably oversampled, and adequate measurement of the evolution would have been possible at 5-20% of the total dose used here.

The time-lapse data reveal some of the complex copper chemistry involved in the protocols, and the formation of both expected and unexpected by-products. The nantokite produced in the protocol tested is contaminated with cuprite and paratacamite as a consequence of the rinsing process (rinsing in water or dilute sodium sesquicarbonate is actually a well recognized conservation treatment which has the intended effect of converting nantokite to passivating cuprite). An alternative protocol due to Faltermeyer[31], which we have also tested, produces nantokite in isolation.

Acknowledgements

The authors acknowledge with thanks the financial support from the Research Foundation - Flanders (FWO), the ESRF through long term project EC188, and the Paul Instrument Fund (eCell construction). We also thank R. A. Grayburn, A. Pappot and G.K.C. Jones for their contribution to the data taking and T. Hase and D. Walker for valuable discussions. The eSpin and eCell equipment used were designed by EVA Surface Analysis and made by Derrick Richards and Adrian Lovejoy in the Physics Department at Warwick University.
Supporting Information Available: This material is available free of charge via the Internet at http://pubs.acs.org.

References

[1] Davenport, A. J.; Ryan, M. P.; Simmonds, M. C.; Ernst, P.; Newman, R. C.; Sutton, S. R. and Colligon, J. S. *J. Electrochem. Soc.* **2001**, 148, B217-B221

[2] Oyanagi, H.; Sun, Z. H.; Jiang, Y.; Uehara, M., Nakamura, H.; Yamashita, K. Zhang, L.; Lee, C.; Fukano, A.; and Maeda, H. *J. Synchrotron Rad*. **2011**, 18, 272-279

[3] Adriaens, A.; Dowsett, M.; Jones, G.K.C.; Leyssens, K.; Nikitenko, S. *J. Anal. At. Spectrom.* **2009**, *24*, 62-68.

[4] Lutzenkirchen-Hecht, D.; and Frahm R. *J. Phys. Chem. B* **2001**, 105, 9988-9993

[5] Monnier, J.; Réguer, S.; Vantelon, D.; Dillmann, P.; Neff, D.; Guillot, I. *Appl. Pnys. A* **2010**, 99, 399-406

[6] Forsberg, J.; Hedberg, J.; Leygraph C. Nordgren J.; and Duda, L. C. *J. Electrochem. Soc*. **2010**, 157, C110-C115

[7] Rayment, T.; Davenport, A. J.; Dent, A. J.; Tinnes, J-P.; Wiltshire, R. J. K.; Martin, C.; Clark, G; Quinn, P.; and Mosselmans, J. F. W. *Electrochem. Commun.* **2008**, 10, 855-858

[8] Lucas, C. A. *Electrochim. Acta* **2002**, 47, 3065-3074

[9] Adriaens, A.; and Dowsett M. *Accounts of Chemical Research* **2010**, 43, 927-935

[10] Frenkel, A.I.; Wang, Q.; Marinkovic, N.; Chen, J. G.; Barrio, L.; Si, R., Lopez-Camara, A.; Estrella, A. M.; Rodriguez, J. A.; Hanson, J. C. *J. Phys. Chem. C* **2011**, 115, 17884-17890

[11] Fleischmann, M.; Hendra, P. J.; Robinson. J. *Nature* 1980, 288, 152-154

[12] Thickett, D.; Odlyha, M. *J. Therm. Anal. Calorim.* **2005**, 80, 565-571.

[13] Scott, D.A.; Copper and Bronze in Art: Corrosion, Colorants, Conservation; The Getty Conservation Institute: Los Angeles, 2002.

[14] Kvashnina, K. O.; Butorin, S. M.; Modin, A.; Soroka, I.; Marcellini, M.; Nordgren J.; Guo, J-H.; Wetme, L. *Chem. Phys. Letts.* **2007**, 447, 54-57

[15] Leyssens, K.; Adriaens, A.; Dowsett, M.; Schotte, B.; Oloff, I.; Pantos, E.; Bell, A.; Thompson, S. *Electrochem. Commun.* **2005**, 7, 1265-1270.

[16] Hughes, R.; Rowe, M. *The Colouring, Bronzing and Patination of Metals*, Thames and Hudson: London, 1982.

[17] Lamy, C. *Stabilisation d'objets archéologiques chloruré en alliage cuivreux*, ARC' Antique internal report: 1997

[18] Cernik, R.J.; Bartnes, P.; Bushnell-Wye, G.; Dent, A.J.; Diakun, G.P.; Flaherty, J.V.; Greaves, G.N.; Heeley, E.L.; Helsby, W.; Jacques, S.D.M.; Kay, J.; Rayment, T.; Ryan, A.; Tang, C.C.; Terrill, N.J. *J. Synch Rad.* **2004**, *11*, 163-170

[19] Brown S.D.; Bouchenoire L.; Bowyer D.; Kervin J.; Laundy D.; Longfield M.J.; Mannix D.; Paul D.F.; Stunault A.; Thompson P.; Cooper M.J.; Lucas C.A.; Stirling W.G. *J. Synch. Rad.* **2001**, *8*, 1172-1181

[20] Lewis, R.A.; Helsby, W.I.; Jones, A.O.; Hall, C.J.; Parker, B.; Sheldon, J.; Clifford, P.; Hillen, M.; Sumner, I.; Fore, N.S.; Jones, R.W.M.; Roberts, K.M. *Nucl. Instrum. Meth.* B **1997**, *392*, 32-41

[21] http://henke.lbl.gov/optical_constants/ accessed 13th April 2012

[22] Dowsett, M.; Adriaens, A. *Anal. Chem*. **2006**, *78,* 3360-3365

[23] http://www2.warwick.ac.uk/fac/sci/physics/research/condensedmatt/sims/esaprojectpublic

[24] http://database.iem.ac.ru/mincryst/index.php

[25] Chichagov, A.V.;Varlamov, D.A.; Dilanyan, R.A.; Dokina, T.N.; Drozhzhina, N.A.; Samokhvalova, O.L.; Ushakovskaya, T.V.; Crystallography Reports **2001**, *46*, 867-879

[26] http://www.icdd.com/

[27] Toney, M. F.; Brennan, S. *Phys. Rev. B* **1989**, *39*, 7963-7966

[28] Wang, Q.; Merkel, J. F. *Studies in Conservation* **2001**, *46*, 242-250

[29] Warraky, A. A.; El-Aziz, A. M.; Soliman, Kh. A. *Anti-Corrosion Methods and Materials* **2007**, *54*, 155-162

[30] McLeod, I. D. *Bronze disease: An electrochemical explanation,* Institute for the Conservation of Cultural Materials (1981) Bulletin 7, 16-26

[31] Faltermeyer, R. B. *Studies in Conservation* **1999**, *44*, 121-128

For TOC only: